MATERIALS CHEMISTRY
FRONTIERS

RESEARCH ARTICLE

View Article Online
View Journal | View Issue

Cite this: *Mater. Chem. Front.*, 2023, **7**, 1841

Blue emitters with various electron-donors attached to the 9-phenyl-9-phosphafluorene oxide (PhFIOP) moiety and their thermally activated delayed fluorescence (TADF) behavior†

Xi Chen,[a] Siqi Liu,[a] Yuling Sun,[a] Daokun Zhong,[a] Zhao Feng,[a] Xiaolong Yang,[a] Bochao Su,[a] Yuanhui Sun,[a] Guijiang Zhou,*[a] Bo Jiao*[b] and Zhaoxin Wu[b]

A series of luminescent molecules have been developed through attaching various electron-donors to the 4- and/or 6-positions of the 9-phenyl-9-phosphafluorene oxide (PhFIOP) moiety. Furthermore, their photophysical, thermal, electrochemical and electroluminescent properties have been characterized in detail. Critically, it has been found that introducing two electron-donors to the 4- and 6-positions of the PhFIOP moiety can furnish a smaller singlet–triplet energy gap (ΔE_{ST}) than the analogues with a single electron-donor at the 4-position of the PhFIOP moiety. Hence, PhFIOP-based emitters with two phenoxazine and two acridine moieties as electron-donors can show thermally activated delayed fluorescence (TADF) behavior with a high reverse inter-system crossing constant (k_{RISC}) in the order of 10^6 s^{-1}. In contrast, TADF features cannot be observed in PhFIOP-based emitters with only one electron-donor. In addition, these luminescent molecules can also exhibit high photoluminescence quantum yields (PLQYs) ranging from 70% to 90% in doped films, which results in excellent electroluminescence (EL) performance. To validate this idea, monochromatic OLED devices have been fabricated and the results show a maximum current efficiency (η_L) of 55.6 cd A^{-1}, a power efficiency (η_P) of 49.2 lm W^{-1}, and an external quantum efficiency (η_{ext}) of 27.3%. Moreover, blue EL emission has also been achieved with CIE (0.17, 0.14) as well as high EL efficiencies of 18.7 cd A^{-1}, 15.6 lm W^{-1}, and 21.9%, respectively. Thus, these PhFIOP-based emitters will enrich the structural diversity of APO-type TADF molecules with high EL efficiency.

Received 22nd December 2022,
Accepted 27th February 2023

DOI: 10.1039/d2qm01339h

rsc.li/frontiers-materials

Introduction

Recently, a remarkable breakthrough in the development of organic light-emitting molecules, the so-called thermally activated delayed fluorescence (TADF) materials, have attracted researchers' interests.[1–5] Compared with traditional fluorescent materials, the generated triplet excitons can be harvested by a reverse intersystem crossing (RISC) process induced by a sufficiently small singlet–triplet energy gap (ΔE_{ST}), thus the TADF materials can achieve 100% exciton utilization efficiency.[6–15] Meanwhile, due to the lack of precious metal ions, TADF materials are more cost-effective and environmentally friendly than phosphorescent complexes.[16,17] Besides, they also possess an excellent electroluminescence efficiency comparable to that of phosphorescent complexes.[18–20] It has been reported that the construction of a donor–acceptor (D–A) structure is a facile way to prepare TADF luminescent molecules.[21–30] Thus, the enrichment of the structure of different donor/acceptor groups is of great importance for the construction of efficient TADF molecules.

Aryl phosphine oxide (APO) units are widely applied in organic optoelectronic molecules due to their excellent electron injection/transport capability.[4,31–36] For example, Rajamalli's team has reported a kind of non-doped green organic light-emitting diodes (OLEDs) with the triphenylphosphine oxide as an electron-acceptor, showing an external quantum efficiency (η_{ext}) over 7.2%, a current efficiency (η_L) of 28.3 cd A^{-1}, and a power efficiency (η_P) of 23.0 lm W^{-1}.[37] Besides, APO-type groups are also commonly introduced into novel organic ligands to construct efficient phosphorescent complexes as well as new efficient host materials.[38–43] With so many excellent

[a] *School of Chemistry, State Key Laboratory for Mechanical Behavior of Materials, Engineering Research Center of Energy Storage Materials and Devices, Ministry of Education, Xi'an Jiaotong University, Xi'an 710049, People's Republic of China. E-mail: zhougj@mail.xjtu.edu.cn*

[b] *Key Laboratory of Photonics Technology for Information, School of Electronic and Information Engineering, Xi'an Jiaotong University, Xi'an 710049, People's Republic of China. E-mail: bojiao@mail.xjtu.edu.cn*

† Electronic supplementary information (ESI) available. See DOI: https://doi.org/10.1039/d2qm01339h

reports, APO-type moieties show great potential for the construction of TADF molecules. Therefore, it is essential to enrich the structural diversity by chemical modifications. Yasuda's team from Kyushu University has introduced the oxygen atom as a bridge-linked atom into the triphenylphosphine group and achieved a maximum η_{ext} of 12.3%.[4] This proves that this approach by locking the two benzene rings of triphenylphosphine can enhance the rigidity of the molecular structure, reduce the non-radiative decay of the molecule, and thus improve the electroluminescence (EL) efficiency. Inspired by this method, more APO-based emitters with improved rigidity have been reported.[32,42,44–49]

Among the APO-type moieties, the 9-phenyl-9-phosphafluorene oxide (PhFIOP) group can possess inherent advantages of a highly rigid structure to furnish improved opto-electronic properties. Recently, we have introduced electron-donors to the 2- and 8-positions of the PhFIOP unit to construct new green TADF emitters showing high electroluminescence (EL) efficiencies of 23.3%, 83.7 cd A^{-1}, 59.1 lm W^{-1} for η_{ext}, η_L, and η_P, respectively, indicating its great potential for developing highly efficient TADF emitters.[50] Unfortunately, TADF emitters with the PhFIOP unit as an electron-acceptor are very scarce, especially blue emitters which are important for full-color displays. Furthermore, construction of a PhFIOP unit involves tedious synthetic processes and very sensitive reagents. So, developing new PhFIOP-based TADF emitters which can be synthesized conveniently is very necessary. Based on the aforementioned content, a series of new PhFIOP-based blue TADF emitters have been synthesized conveniently *via* successive nucleophilic aromatic substitution (S_NAr) reactions between dibenzothiophene dioxides and $PhPH_2$-KOH under very mild reaction conditions. Furthermore, various electron-donors have been introduced to the 4- and/or 6-positions of the PhFIOP moiety to optimize their TADF behaviors. Encouragingly, these new PhFIOP-based TADF emitters can show impressive blue EL performances. Obviously, this research can provide crucial information for developing novel PhFIOP-based TADF emitters for OLED applications.

Experimental

General information

Commercial materials are used directly in the reaction without pretreatment, and all reactions were carried out in a nitrogen atmosphere using Schlenk techniques. All the reactions are monitored by thin-layer chromatography (TLC) sheets from Merck In. The products are separated and purified by column chromatography and preparative TLC plates which are conducted using silica gel from Shanghai Qingdao (300–400 mesh). The ultraviolet-visible (UV-vis) and photoluminescence (PL) spectra of all compounds are obtained using a PerkinElmer Lambda 950 spectrophotometer and Edinburgh Instruments FLS920 fluorescence spectrophotometer at room temperature, respectively. ^1H, ^{13}C, and ^{31}P NMR spectra are obtained using a Bruker Avance 400 or 600 MHz NMR spectrometer, and $CDCl_3$ is selected as the solvent. Thin film spectra and lifetimes of TADF emitters are measured using an Edinburgh FLS920 fluorescence spectrometer. Absolute photoluminescence quantum yields (PLQYs) of solution samples and doped films are obtained using an integrating sphere. Fast atom bombardment mass spectrometry (FAB-MS) spectra are obtained on a Finnigan MAT SSQ710 system. Cyclic voltammetry measurements are carried out at a scan rate of 100 mV s^{-1} on a Princeton Applied Research model 2273A potentiostat through a three-electrode configuration with a glassy carbon working electrode, a Pt-sheet counter electrode, and a Pt-wire reference electrode in the electrolyte of 0.1 M $[Bu_4N]PF_6$ in degassed CH_3CN. All potentials are quoted with reference to the ferrocene/ferrocenium (Fc/Fc^+) couple as an internal calibrant.

Synthesis

Preparation details of the key intermediate compounds, 4-bromodibenzo[*b*,*d*]thiophene-5,5-dioxide, 4,6-dibromodibenzo-[*b*,*d*]thiophene-5,5-dioxide, **PhSO-*o*-Oz**, **PhSO-*o*-Ad**, **PhSO-*o*-Cz**, **PhSO-*o*-2Oz**, **PhSO-*o*-2Ad**, and **PhSO-*o*-2Cz**, followed the reported literature[51–55] and their synthetic details are presented in the ESI.†

Specific procedure for the synthesis of PhFIOP-based emitters

FIOP-*o*-Oz. Under a nitrogen atmosphere, **PhSO-*o*-Oz** (1.0 equiv., 0.10 g, 0.21 mmol), phenylphosphine (2.0 equiv., 0.02 g, 0.42 mmol), and KOH (3.0 equiv., 0.03 g, 0.63 mmol) are added to a solution of DMSO (5 mL) and then the mixture is stirred for 12 h at 50 °C. After the reaction, the reaction mixture is cooled to room temperature and then H_2O_2 (2 mL) is added dropwise. After stirring for 2 h, water (20 mL) is added, and then the reaction mixture is extracted with CH_2Cl_2 (30 mL) three times and dried with anhydrous Na_2SO_4. After evaporation to dryness, the residue is purified by column chromatography over silica gel using AcOEt/petroleum ether (1 : 2, v : v) as the eluent with a high yield of 80%. The product is obtained as a white solid.

FIOP-*o*-Ad. PhSO-*o*-Ad (1.0 equiv., 0.10 g, 0.20 mmol), phenylphosphine (2.0 equiv., 0.02 g, 0. 40 mmol), KOH (3.0 equiv., 0.02 g, 0.60 mmol) and DMSO (5 mL) are added into 10 mL Schlenk tubes in a nitrogen atmosphere and stirred vigorously for 12 h at 50 °C. When the reaction is finished, the reaction mixture is cooled to room temperature and H_2O_2 (2 mL) is added dropwise. After stirring for 2 h, water (20 mL) is added, and then the reaction mixture is extracted with CH_2Cl_2 (30 mL) three times and dried with anhydrous Na_2SO_4. After evaporation to dryness, the residue is purified by column chromatography over silica gel using AcOEt/petroleum ether (1 : 2, v : v) as the eluent with a high yield of 83%. **FIOP-*o*-Ad** appears as a white solid.

FIOP-*o*-Cz. Under a nitrogen atmosphere, **PhSO-*o*-Cz** (1.0 equiv, 0.10 g, 0.20 mmol), phenylphosphine (2.0 equiv, 0.02 g, 0.40 mmol), and KOH (3.0 equiv, 0.02 g, 0.60 mmol) are added into DMSO (5 mL) and then the mixture is heated to 50 °C and stirred for 12 h. After the reaction is accomplished, the reaction mixture is cooled to room temperature and H_2O_2 (2 mL) is added dropwise. After stirring for 2 h, water (20 mL) is added, and then the reaction mixture is extracted with CH_2Cl_2 (30 mL) three times and dried with anhydrous Na_2SO_4.

After evaporation to dryness, the residue is purified by column chromatography over silica gel using AcOEt/petroleum ether (1 : 2, v : v) as the eluent with a high yield of 82%. The product is obtained as a white solid.

FIOP-*o*-2Oz. Under a nitrogen atmosphere, **PhSO-*o*-2Oz** (1.0 equiv, 0.10 g, 0.14 mmol), phenylphosphine (4.0 equiv, 0.06 g, 0.56 mmol), and KOH (3.0 equiv, 0.02 g, 0.42 mmol) were added into a solution of DMSO (5 mL) and then the mixture is stirred for 12 h at 50 °C. The reaction mixture was cooled to room temperature after the reaction and H_2O_2 (4 mL) was added dropwise. After stirring for 2 h, water (20 mL) is added to the system, and then the reaction mixture is extracted with CH_2Cl_2 (40 mL) three times and dried with anhydrous Na_2SO_4. After evaporation to dryness, the residue is purified by column chromatography over silica gel using CH_2Cl_2/petroleum ether (2 : 1, v : v) as the eluent with a yield of 54%. The product is a white solid.

FIOP-*o*-2Ad. **PhSO-*o*-2Ad** (1.0 equiv., 0.10 g, 0.13 mmol), phenylphosphine (4.0 equiv., 0.06 g, 0.52 mmol), and KOH (3.0 equiv., 0.02 g, 0.39 mmol) are added to a solution of DMSO (5 mL) in a nitrogen atmosphere and then the mixture is stirred for 12 h at 50 °C. After the reaction, the reaction mixture is cooled to room temperature and H_2O_2 (4 mL) is added dropwise. After stirring for 2 h, water (20 mL) is added, and then the reaction mixture is extracted with CH_2Cl_2 (40 mL) three times and dried with anhydrous Na_2SO_4. After evaporation to dryness, the residue is purified by column chromatography over silica gel using CH_2Cl_2/petroleum ether (2 : 1, v : v) as the eluent with a yield of 52%. The product is obtained as a white solid.

FIOP-*o*-2Cz. Under a nitrogen atmosphere, **PhSO-*o*-2Cz** (1.0 equiv., 0.10 g, 0.14 mmol), phenylphosphine (4.0 equiv., 0.06 g, 0.56 mmol), and KOH (3.0 equiv., 0.02 g, 0.42 mmol) are added to a solution of DMSO (5 mL) and then stirred for 12 h at 50 °C. The system is cooled to room temperature after the reaction is accomplished and H_2O_2 (4 mL) is added dropwise. After stirring for 2 h, water (20 mL) is added, and then extracted with CH_2Cl_2 (40 mL) three times and dried with anhydrous Na_2SO_4. After evaporation to dryness, the residue is purified by column chromatography over silica gel using CH_2Cl_2/petroleum ether (2 : 1, v : v) as the eluent with a yield of 51%. **FIOP-*o*-2Cz** also appears white.

FIOP-*o*-Oz. ^{1}H NMR (400 MHz, $CDCl_3$, δ): 7.91–7.88 (m, 2H), 7.79 (dt, J = 8.0, 4.0 Hz, 2H), 7.73–7.59 (m, 3H), 7.46–7.26 (m, 7H), 7.20 (td, J = 8.0, 4.0 Hz, 2H), 6.76–6.56 (m, 6H), 5.82 (dd, J = 7.6, 1.6 Hz, 2H); ^{13}C NMR (101 MHz, $CDCl_3$, δ): 145.82, 145.74, 144.05, 143.02, 142.80, 141.77, 141.56, 139.53, 138.70, 134.34, 133.80, 133.51, 132.22, 131.87, 131.18, 131.07, 130.51, 130.43, 130.04, 129.94, 129.81, 128.29, 128.17, 123.37, 123.24, 121.35, 121.25, 120.44, 120.34, 115.52, 113.35; ^{31}P NMR (162 MHz, $CDCl_3$, δ): 34.93; FAB-MS (m/z): 533 [M]+; anal. calcd for $C_{36}H_{24}NO_2P$: C, 81.04; H, 4.53; N, 2.63. Found: C, 81.12; H, 4.48; N, 2.71.

FIOP-*o*-Ad. ^{1}H NMR (400 MHz, $CDCl_3$, δ): 7.92–7.89 (m, 2H), 7.84 (dt, J = 8.0, 4.0 Hz, 2H), 7.74–7.67 (m, 2H), 7.64 (t, J = 7.6 Hz, 1H), 7.50–7.34 (m, 7H), 7.31–7.27 (m, 2H), 7.23 (dd, J = 8.0, 2.0 Hz, 2H), 7.00 (td, J = 8.0, 1.6 Hz, 2H), 6.94 (td, J = 8.0, 1.2 Hz, 2H), 6.18 (dd, J = 8.0, 1.2 Hz, 2H), 1.69 (s, 6H); ^{13}C NMR (101 MHz, $CDCl_3$, δ): 140.99, 140.91, 133.75, 133.47, 131.89, 131.87, 131.23, 131.12, 131.03, 130.68, 130.59, 130.13, 130.05, 129.95, 129.89, 129.78, 128.34, 128.21, 126.37, 125.25, 121.32, 121.22, 120.65, 120.36, 120.27, 114.15, 42.77, 36.07, 31.24; ^{31}P NMR (162 MHz, $CDCl_3$, δ): 35.01; FAB-MS (m/z): 559 $[M]^+$; anal. calcd for $C_{39}H_{30}NOP$: C, 83.70; H, 5.40; N, 2.50. Found: C, 83.65; H, 5.49; N, 2.53.

FIOP-*o*-Cz. ^{1}H NMR (400 MHz, $CDCl_3$, δ): 8.17 (d, J = 8.0 Hz, 2H), 7.91 (t, J = 8.0 Hz, 2H), 7.75 (t, J = 8.0 Hz, 2H), 7.70 (t, J = 7.6 Hz, 2H), 7.65 (t, J = 7.6 Hz, 1H), 7.52 (d, J = 8.0 Hz, 2H), 7.49–7.39 (m, 6H), 7.36–7.30 (m, 5H), 7.19 (dt, J = 7.6, 4.0 Hz, 2H); ^{13}C NMR (101 MHz, $CDCl_3$, δ): 145.91, 142.79, 142.58, 141.99, 141.78, 140.84, 138.41, 137.48, 133.75, 133.54, 131.96, 131.04, 130.45, 130.04, 129.79, 129.51, 128.33, 126.60, 126.05, 123.52, 121.37, 121.27, 120.46, 120.35, 120.25, 120.12, 109.89; ^{31}P NMR (162 MHz, $CDCl_3$, δ): 34.95; FAB-MS (m/z): 517 $[M]^+$; anal. calcd for $C_{36}H_{24}NOP$: C, 83.54; H, 4.67; N, 2.71. Found: C, 83.44; H, 4.72; N, 2.67.

FIOP-*o*-2Oz. ^{1}H NMR (400 MHz, $CDCl_3$, δ): 8.14 (d, J = 7.6 Hz, 6H), 7.98 (dd, J = 7.6, 2.0 Hz, 3H), 7.76 (td, J = 8.0, 1.2 Hz, 3H), 7.73–7.67 (dt, J = 8.0, 4.0 Hz, 6H), 7.49–7.46 (m, 4H), 7.45–7.38 (m, 12H), 7.35–7.27 (m, 12H), 7.24–7.15 (m, 5H), 7.03 (td, J = 8.0, 2.0 Hz, 3H); ^{13}C NMR (151 MHz, $CDCl_3$, δ): 145.47, 145.41, 143.90, 142.57, 142.43, 139.24, 139.22, 139.00, 138.45, 137.86, 136.51, 135.72, 134.18, 133.66, 132.66, 132.13, 132.06, 130.86, 130.79, 130.73, 130.23, 129.32, 129.02, 128.63, 128.21, 127.68, 127.60, 125.28, 123.35, 123.07, 121.40, 121.28, 120.65, 120.37, 115.37, 113.48, 113.19; ^{31}P NMR (162 MHz, $CDCl_3$, δ): 35.70; FAB-MS (m/z): 790 $[M]^+$; anal. calcd for $C_{54}H_{35}N_2O_3P$: C, 82.01; H, 4.46; N, 3.54. Found: C, 82.10; H, 4.53; N, 3.49.

FIOP-*o*-2Ad. ^{1}H NMR (400 MHz, $CDCl_3$, δ): 7.97 (dd, J = 7.6, 2.0 Hz, 2H), 7.81–7.66 (m, 6H), 7.43 (dd, J = 8.0, 4.0 Hz, 2H), 7.25–7.08 (m, 7H), 7.02 (td, J = 7.9, 3.2 Hz, 2H), 6.73–6.51 (m, 12H), 5.72 (d, J = 4.0 Hz, 4H), 1.25 (s, 12H); ^{13}C NMR (151 MHz, $CDCl_3$, δ): 145.71, 145.66, 142.64, 142.50, 141.78, 139.25, 139.06, 136.31, 135.89, 133.64, 132.73, 131.94, 131.64, 131.42, 131.00, 130.93, 130.79, 130.15, 130.01, 129.06, 128.58, 128.25, 127.82, 127.73, 126.52, 126.27, 125.12, 125.06, 120.66, 120.54, 120.39, 120.32, 114.32, 114.07, 35.97, 31.12; ^{31}P NMR (162 MHz, $CDCl_3$, δ): 35.64, FAB-MS (m/z): 843 $[M]^+$; anal. calcd for $C_{60}H_{47}N_2OP$: C, 85.49; H, 5.62; N, 3.32. Found: C, 85.57; H, 5.58; N, 3.26.

FIOP-*o*-2Cz. ^{1}H NMR (400 MHz, $CDCl_3$, δ): 7.98 (dd, J = 7.6, 2.0 Hz, 2H), 7.80 (dt, J = 8.0, 2.0 Hz, 4H), 7.75 (td, J = 8.0, 1.2 Hz, 2H), 7.49 (dd, J = 7.2, 4.0 Hz, 2H), 7.47–7.40 (m, 4H), 7.25–7.17 (m, 6H), 7.10 (td, J = 8.0, 2.0 Hz, 2H), 6.98–6.90 (m, 9H), 6.09 (dd, J = 7.6, 1.6 Hz, 4H); ^{13}C NMR (151 MHz, $CDCl_3$, δ): 145.69, 145.63, 142.67, 142.53, 140.72, 140.58, 139.26, 138.39, 138.20, 137.26, 135.71, 135.22, 133.71, 132.78, 132.25, 131.91, 131.59, 131.21, 131.14, 131.03, 130.87, 130.66, 130.63, 130.55, 129.59, 129.06, 128.89, 128.25, 127.88, 127.79, 126.89, 126.80, 126.40, 126.03, 125.89, 125.32, 123.56, 123.39, 120.59, 120.40, 120.32, 120.29, 120.16, 120.00, 110.09, 109.81; ^{31}P NMR (162 MHz, $CDCl_3$, δ): 35.90; FAB-MS (m/z): 758 $[M]^+$; anal. calcd for $C_{54}H_{35}N_2OP$: C, 85.47; H, 4.65; N, 3.69. Found: C, 85.52; H, 4.58; N, 3.74.

Results and discussion

Synthesis and structural characterization

Synthetic strategies for the PhFIOP-based emitters are summarized in Scheme 1 and details of the synthetic methods for intermediates are provided in the ESI.† In order to synthesize target molecules, aromatic boron with electron-donors need to be prepared first by Ullman and Suzuki cross-coupling reactions. The synthesis of the target molecules starts from 4-bromodibenzo[*b*,*d*]thiophene and 4,6-dibromodibenzo[*b*,*d*]thiophene,

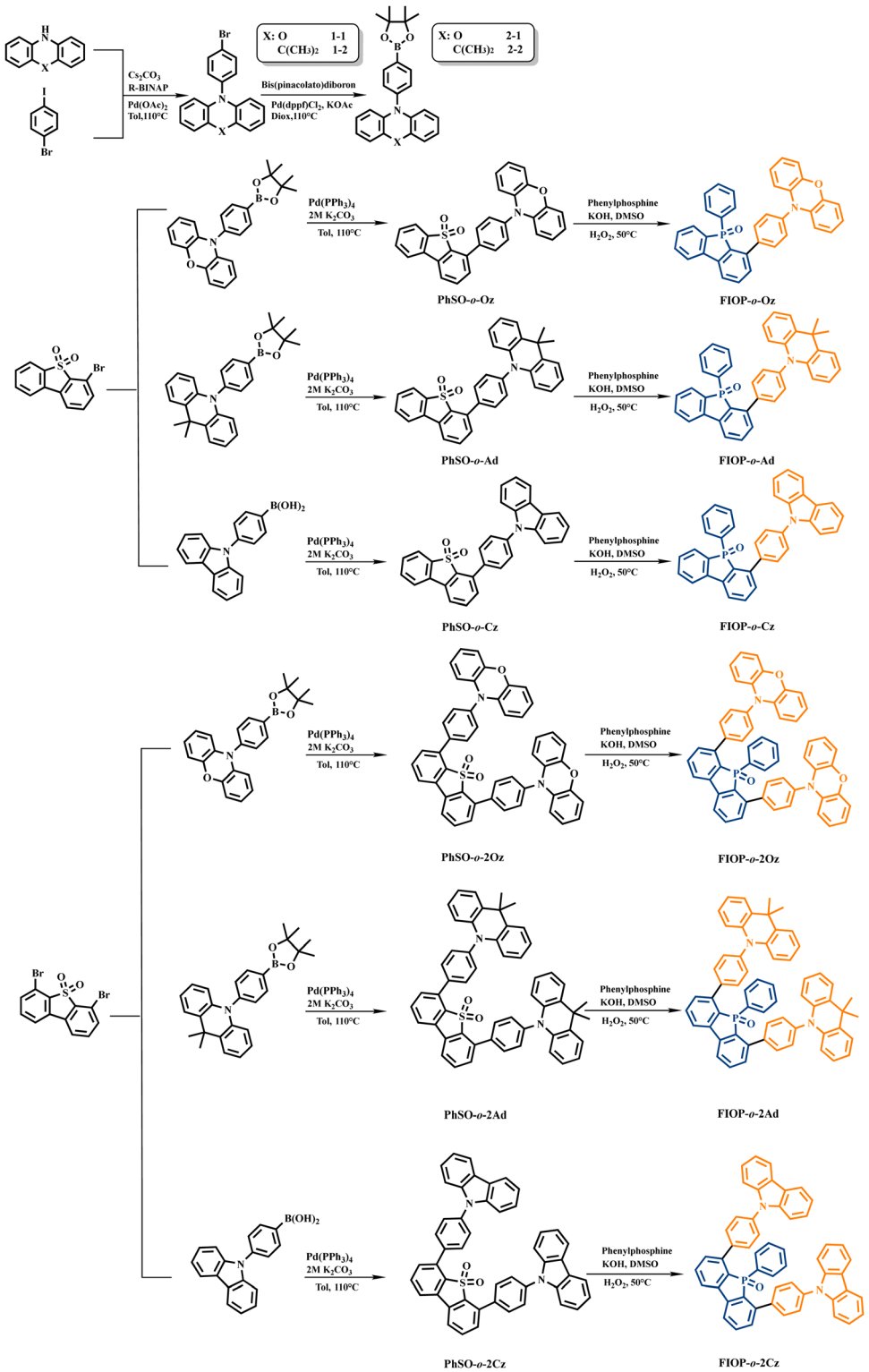

Scheme 1 Synthesis of the PhFIOP-based emitters.

followed by oxidation and Suzuki cross-coupling with aromatic borons with electron-donors to obtain the precursors **PhSO-*o*-Oz**, **PhSO-*o*-Ad**, **PhSO-*o*-Cz**, **PhSO-*o*-2Oz**, **PhSO-*o*-2Ad**, and **PhSO-*o*-2Cz**. Then, they undergo successive nucleophilic aromatic substitution (S_NAr) reactions with $PhPH_2$-KOH under very mild reaction conditions and then oxidation with H_2O_2 at room temperature to obtain the final product. **FIOP-*o*-Oz**, **FIOP-*o*-Ad**, and **FIOP-*o*-Cz** of the D–A structure with a single electron-donor can be synthesized in high yields of around 80%, while **FIOP-*o*-2Oz**, **FIOP-*o*-2Ad**, and **FIOP-*o*-2Cz** of the D–A–D structure containing two electron-donors show slightly lower yields of around 50%, probably due to the higher steric hindrance in the *ortho*-positions of the P=O center. It is worth mentioning that this method of constructing a PhFIOP moiety is very mild without the use of sensitive organometallic reagents and in higher yields than the conventional strategy,[56–58] which provides a new idea for the synthesis of PhFIOP-based emitters.

The chemical structures of these PhFIOP-based emitters have been characterized. According to the NMR spectra of these compounds, there appears all the characteristic signals of the corresponding groups, which confirms the accuracy of the synthesis (Fig. S1–S6, ESI†). From the ^{1}H NMR spectra, a set of signals at *ca.* 6.60 ppm to 5.80 ppm and *ca.* 7.16 ppm to 7.01 ppm are ascribed to the phenoxazine units of **FIOP-*o*-Oz** and **FIOP-*o*-2Oz**, respectively. The singlet peak at 1.69 ppm is attributed to the methyl groups of the acridine unit in **FIOP-*o*-Ad**. Similarly, the singlet peak signal at 1.25 ppm belongs to the acridine units in **FIOP-*o*-2Ad**. The characteristic peak signals of the carbazole moiety in **FIOP-*o*-Cz** appears at *ca.* 7.19 ppm. Due to the structural similarity, the ^{31}P NMR spectra of all the emitters show a distinct characteristic signal around 35.00 ppm, which are assigned to the PhFIOP group.

Thermal and photophysical properties

Thermal properties of the PhFIOP-based emitters are characterized *via* thermogravimetric analysis (TGA) under a nitrogen flow and the data are summarized in Table 1. All these emitters possess excellent thermal stability with a high thermal decomposition temperature (T_d) ranging from 321 to 424 °C, which is important for the preparation of OLEDs. At the same time, due to the improved structural rigidity of the emitters containing two electron-donors, their thermal decomposition temperature is significantly higher than that with one electron-donor. From their TGA curves (Fig. S7, ESI†), it should be noted that the weight-loss of **FIOP-*o*-Oz** and **FIOP-*o*-Cz** should probably result from their sublimation, and thus their T_d may be even higher than the data revealed by their TGA curves. However, as for **FIOP-*o*-Ad** and **FIOP-*o*-2Ad**, they seem to begin to decompose at a lower temperature because of the less rigidity of the acridine groups.

Fig. 1 shows the UV-vis absorption spectra of the PhFIOP-based emitters in toluene at 293 K and the corresponding data are included in Table 1. The UV spectra suggest that all these emitters exhibit two absorption peaks at *ca.* 350 nm and *ca.* 400 nm. The high-energy absorption band is attributed to $\pi \rightarrow \pi^*$ transitions in the electron-donor and electron-acceptor, while the low-energy absorption band should be ascribed to intramolecular charge-transfer transition. It is noteworthy that the absorption spectral profile does not change obviously after introduction of the second electron-donor, probably due to the insignificant effect on the electron transition of these PhFIOP-based emitters. However, by varying the electron-donating abilities of the electron-donor, their absorption spectra can exhibit obvious differences (Fig. 1).

In order to gain insight into the absorption behavior of these PhFlOP-based emitters, key frontier molecular orbitals (MOs) based on the ground states (S_0) have been obtained by theoretical calculation (Fig. 2). From the MO diagram, it can be noticed that the highest occupied molecular orbital (HOMO) and the lowest unoccupied molecular orbital (LUMO) are clearly separated, and the HOMOs are mainly located on the π orbitals of the electron-donors, while LUMOs are mainly distributed in the π^* orbitals of the PhFIOP unit. Hence, the electron transition process with the lowest energy exhibits an obvious intramolecular charge transfer (CT) feature, so the low-energy absorption band of these PhFlOP-based emitters should be induced by the intramolecular CT transition. Among all the electron-donors, the phenoxazine group possesses the strongest electron-donating ability to facilitate a CT transition. Therefore, **FIOP-*o*-Oz** and **FIOP-*o*-2Oz** can show the intramolecular CT absorption band with the lowest energy-level, indicated by their absorption onset at *ca.* 410 nm. Owing to the much weaker electron-donating ability of the carbazole moiety, **FIOP-*o*-Cz** and **FIOP-*o*-2Cz** should show the intramolecular CT absorption band with the highest energy-level, indicated by their absorption onset at the shortest wavelength *ca.* 370 nm.

Table 1 Photophysical and thermal data of these PhFIOP-based emitters

Compound	Absorption[a] λ_{abs} (nm)	Emission λ_{em} (nm) solution[b]/film[c]	PLQY solution[d]/film[e]	T_d[f] (°C)
FIOP-*o*-Oz	286(4.46), 299(4.40), 331(4.45), 396(3.65)	496/495	90.2%/93.3%	363
FIOP-*o*-Ad	286(4.45), 298(4.32), 340(3.54), 376(2.00)	455/453	80.4%/80.0%	352
FIOP-*o*-Cz	295(4.38), 315(4.28), 328(4.29), 341(4.27), 373(3.03)	400/405	82.1%/81.2%	321
FIOP-*o*-2Oz	284(4.55), 291(4.48), 302(4.45), 328(4.55), 392(3.68)	497/503	73.2%/65.6%	415
FIOP-*o*-2Ad	284(4.53), 292(4.46), 344(3.53), 378(2.18)	451/456	93.3%/96.5%	397
FIOP-*o*-2Cz	287(4.37), 294(4.45), 327(4.15), 341(4.13), 379(3.13)	403/418	69.84%/73.31%	424

[a] Measured at a concentration of *ca.* 10^{-5} M in toluene at room temperature, and log ε values are presented in parentheses. [b] Measured in toluene at 293 K. [c] Measured in the doped mCP film (doping ratio: 10 wt %) at 293 K. [d] Absolute PLQY in toluene measured with an integrating sphere at room temperature. [e] Absolute PLQY in the doped mCP film (doping ratio: 10 wt %) measured with an integrating sphere at 293 K. [f] T_d is the decomposition temperature.

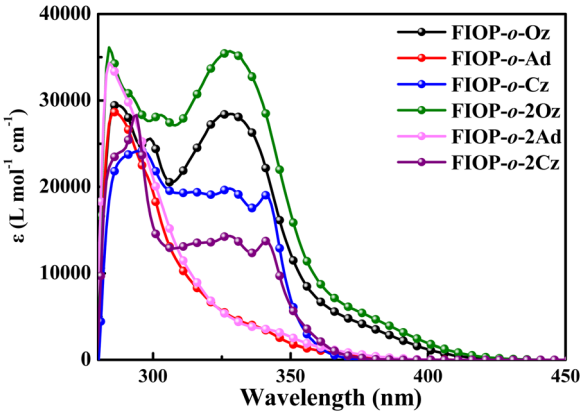

Fig. 1 UV-vis absorption spectra of these PhFIOP-based emitters measured in toluene at 293 K.

With a stronger electron-donating ability than carbazole moiety, the acridine unit can afford a lower energy-level for the intramolecular CT absorption band to **FIOP-*o*-Ad** and **FIOP-*o*-2Ad**, showing absorption onset at a longer wavelength *ca.* 380 nm. From Fig. 2, we can see that both mono- and di-substituted emitters with the same electron-donor can display very similar HOMO and LUMO patterns to furnish their similar absorption spectral profile (Fig. 1).

Photoluminescence (PL) spectra of these PhFIOP-based emitters are recorded in toluene and in the doped 1, 3-bis(*N*-carbazolyl)benzene (mCP) film (doping ratio: 10 wt%) at 293 K, respectively (Fig. 3). The PhFIOP-based emitters exhibit different emission wavelengths due to the various electron-donating abilities of the electron-donors. The sky-blue emission wavelength of **FIOP-*o*-Oz** and **FIOP-*o*-2Oz** is 496 nm due to the strong electron-donating ability of the phenoxazine moiety. As for **FIOP-*o*-Cz** and **FIOP-*o*-2Cz**, owing to the weaker electron-donating ability of the carbazole group, they show emission maximum at *ca.* 400 nm, showing a blue-shift effect compared with that of the blue-emitting **FIOP-*o*-Ad** and **FIOP-*o*-2Ad** (*ca.* 450 nm) possessing an acridine unit with a stronger electron-donating feature (Fig. 3). Clearly, the emission wavelengths of these PhFlOP-based emitters exhibit good consistence with the energy-levels of their intramolecular CT absorption bands. Hence, it seems that their emission can exhibit an intramolecular CT feature which has been indicated by the structureless PL spectral profiles shown in Fig. 3. From the PL spectra in toluene, it is obvious that the PhFIOP-based emitters containing one or two electron-donors exhibit similar emission behavior. The PL spectra in the doped mCP film are consistent with those in toluene. However, the emission wavelength of **FIOP-*o*-2Cz** in doped film has a slight red shift compared with that in the solution, which may be due to the fact that more rigid planar carbazole units can induce stronger molecular interaction resulting in red-shifted emission. It should be noted that these PhFIOP-based blue emitters show PLQYs ranging from 65% to 90% both in degassed toluene and doped films due to the rigid PhFIOP unit which can restrain the nonradiative decay processes. Especially for **FIOP-*o*-Oz** and **FIOP-*o*-2Ad**, they achieve high PLQYs of 90.2% and 93.3% in toluene, respectively.

TADF behaviors

In order to characterize the TADF behavior of these PhFIOP-based emitters, both the transient decay curves in the doped mCP film (doping ratio: 10 wt%) (Fig. 4) together with those at different temperatures in degassed toluene (Fig. 4, inset) have been obtained. For **FIOP-*o*-2Oz** and **FIOP-*o*-2Ad**, two decay processes are observed in their transient PL decay curves, in both doped mCP film and degassed toluene. The prompt decay shows short lifetimes in the order of nanosecond (29.6 ns for

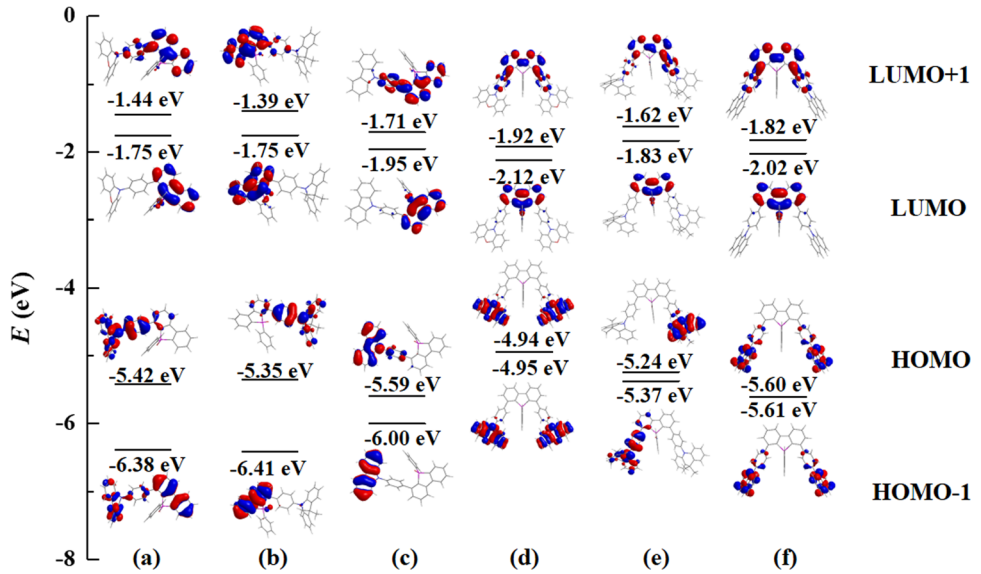

Fig. 2 MO patterns (isocontour value = 0.030) for the PhFIOP-based emitters based on their optimized S_0 geometries. (a) **FIOP-*o*-Oz**, (b) **FIOP-*o*-Ad**, (c) **FIOP-*o*-Cz**, (d) **FIOP-*o*-2Oz**, (e) **FIOP-*o*-Ad**, and (f) **FIOP-*o*-2Cz**.

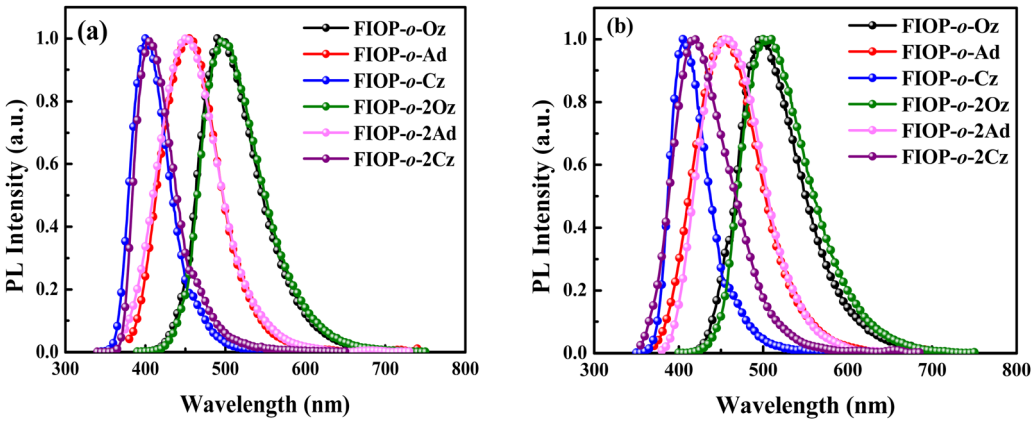

Fig. 3 PL spectra of these PhFIOP-based emitters. (a) Measured in toluene at 293 K, and (b) measured in the doped mCP film (doping ratio: 10 wt %) at 293 K.

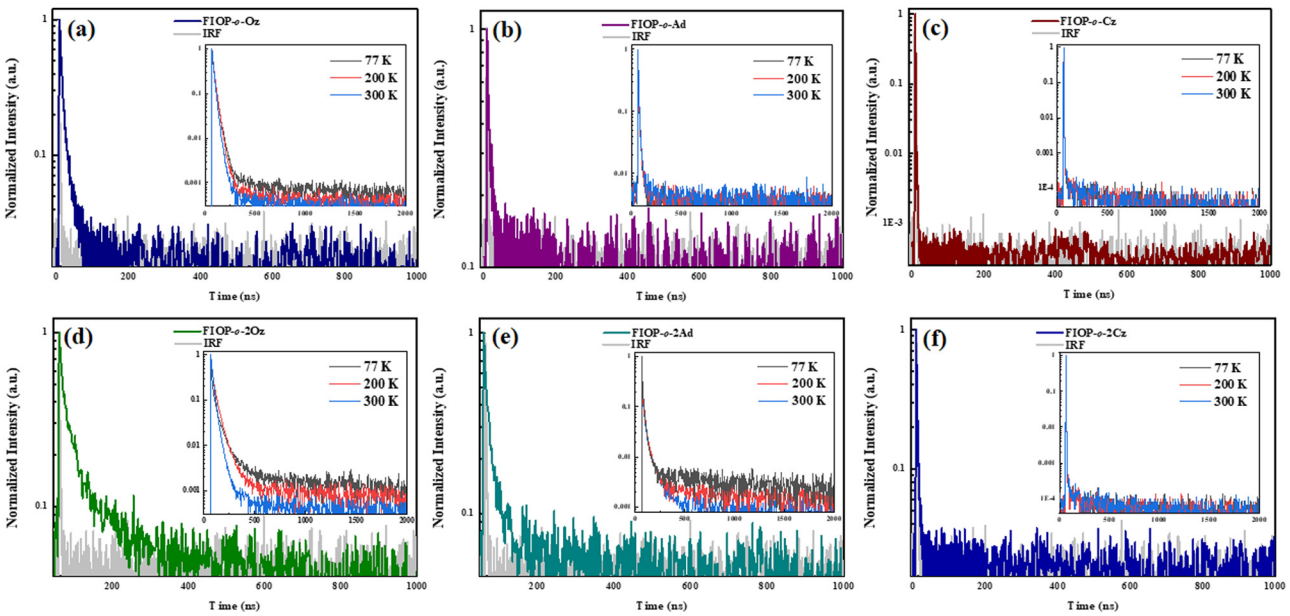

Fig. 4 Transient PL decays for these PhFIOP-based emitters doped in the mCP film (doping ratio: 10 wt %). The inset shows the temperature dependence of transient PL decay in degassed toluene. (a) **FIOP-*o*-Oz**, (b) **FIOP-*o*-Ad**, (c) **FIOP-*o*-Cz**, (d) **FIOP-*o*-2Oz**, (e) **FIOP-*o*-2Ad**, and (f) **FIOP-*o*-2Cz**. IRF: the instrument response functions of the light source.

FIOP-*o*-2Oz and 12.6 ns for **FIOP-*o*-2Ad**), while the delayed decay has a lifetime more than ten times that of the prompt decay (170 ns for **FIOP-*o*-2Oz** and 180 ns for **FIOP-*o*-2Ad**) (Table 2). At the same time, the lifetime of the delayed decay decreases with the increase of temperature, which also reflects the obvious TADF feature. Unfortunately, **FIOP-*o*-Oz**, **FIOP-*o*-Ad**, **FIOP-*o*-Cz** and **FIOP-*o*-2Cz** do not exhibit obvious TADF behavior.

To further interpret the TADF behavior of these PhFIOP-based emitters, natural transition orbital (NTO) patterns for $S_0 \rightarrow S_1$ excitations based on their optimized S_1 geometries have been obtained (Fig. 5). For the PhFIOP-based emitters that contain one electron-donor, they all possess a large ΔE_{ST} (0.406 eV for **FIOP-*o*-Oz**, 0.302 eV for **FIOP-*o*-Ad** and 0.420 eV for **FIOP-*o*-Cz**), which is unfavorable to exhibit TADF behavior. This result is consistent with the transient PL decays. After introduction of the second electron-donor, the torsion angle between the electron-donor and electron-acceptor becomes larger, which promotes the separation of the HOMO and LUMO to achieve a smaller ΔE_{ST}. As for **FIOP-*o*-2Oz**, the results from the theoretical calculations show that the hole and particle orbitals are well separated. In addition, the calculated ΔE_{ST} of **FIOP-*o*-2Oz** is 0.003 eV with a larger twisting angle between its electron-donor and electron-acceptor (79.48°) compared with **FIOP-*o*-Oz** (65.90°). These results indicate that **FIOP-*o*-2Oz** will exhibit a typical TADF behavior, and the same is true for **FIOP-*o*-2Ad**. However, **FIOP-*o*-2Cz** possesses poor separation between its hole and particle orbitals together with a large

Table 2 TADF data of these PhFIOP-based emitters

Compound	S_1[a] (eV)	T_1[a] (eV)	ΔE_{ST}[b] (eV)	τ_{PF}[c] (ns)	τ_{DF}[c] (μs)	Φ_{PF}[d] (%)	Φ_{DF}[d] (%)	k_{PF}[e] (10^7 s^{-1})	k_{DF}[e] (10^5 s^{-1})	k_{ISC}[f] (10^6 s^{-1})	k_{RISC}[f] (10^6 s^{-1})
FIOP-*o*-Oz	2.86	2.54	0.32	14.2							
FIOP-*o*-Ad	3.02	2.66	0.36	8.7							
FIOP-*o*-Cz	3.26	3.04	0.22	7.9							
FIOP-*o*-2Oz	2.62	2.53	0.09	29.6	0.17	27.9	37.0	0.9	21.7	5.4	5.1
FIOP-*o*-2Ad	2.89	2.71	0.18	12.6	0.18	46.9	46.1	3.9	25.6	19.0	4.9
FIOP-*o*-2Cz	3.22	2.88	0.34	3.2							

[a] Experimental data were determined from the onsets of the fluorescence and phosphorescence (77 K) spectra (Fig. S8, ESI) in the doped mCP film (doping ratio: 10 wt%). [b] $\Delta E_{ST} = E_{S1} - E_{T1}$. [c] The prompt fluorescence lifetime (τ_{PF}) and delayed fluorescence lifetime (τ_{DF}) were measured in the doped mCP film at 293 K. [d] The prompt fluorescence quantum yields (Φ_{PF}) and delayed fluorescence quantum yields (Φ_{DF}) were estimated according to the prompt and delayed proportions in transient decay curves. [e] The rate constants of PF and DF (k_{PF} and k_{DF}) evaluated according to experimental data: $k_{PF} = \Phi_{PF}/\tau_{PF}$ and $k_{DF} = \Phi_{DF}/\tau_{DF}$. [f] The rate constants of intersystem crossing and reverse (k_{ISC} and k_{RISC}) are further estimated according to $k_{ISC} = \Phi_{DF}\, k_{PF}/(\Phi_{PF} + \Phi_{DF})$ and $k_{RISC} = k_{DF}\, k_{PF}\, \Phi_{DF}/(k_{ISC}\, \Phi_{PF})$.

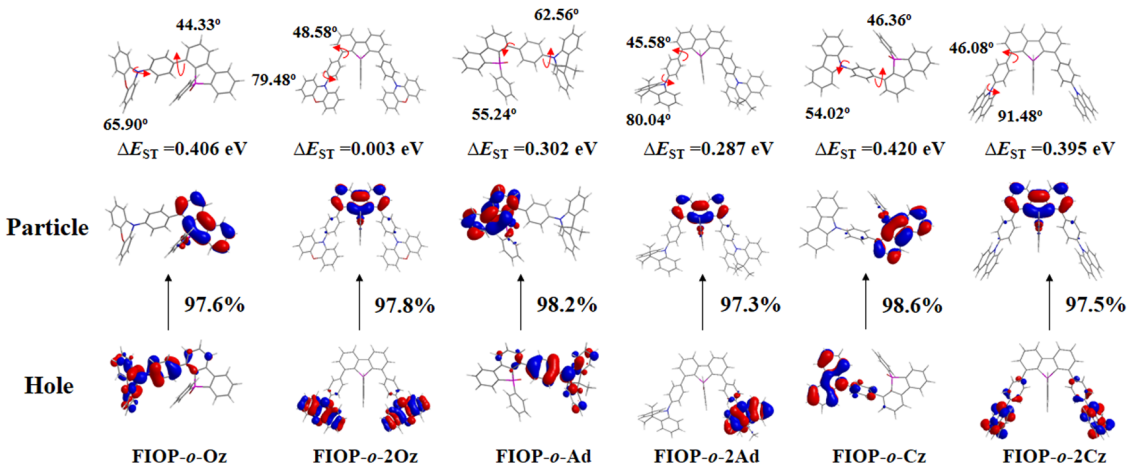

Fig. 5 NTO patterns (isocontour value = 0.030) for $S_0 \rightarrow S_1$ excitations based on the optimized S_1 geometries, together with the S_0 geometry showing the twisting angle between the donor and the acceptor.

ΔE_{ST} (0.395 eV), which should be detrimental to show a TADF effect. Furthermore, the ΔE_{ST} of these PhFIOP-based emitters are also measured experimentally and the data are listed in Table 2. Clearly, the ΔE_{ST} of **FIOP-*o*-2Oz** and **FIOP-*o*-2Ad** is just 0.09 eV and 0.18 eV, respectively, while the data associated with other emitters are obviously much larger (Table 2). This result is consistent with the theoretical calculations. Besides, both **FIOP-*o*-2Oz** and **FIOP-*o*-2Ad** have a high k_{RISC} in the order of 10^6 s^{-1}, which is another key parameter to determine the TADF behavior. This high k_{RISC} indicates the presence of an efficient reverse intersystem crossing process within **FIOP-*o*-2Oz** and **FIOP-*o*-2Ad**, promoting their TADF behavior effectively.

Electrochemical properties

The electrochemical properties of these PhFIOP-based emitters are characterized by cyclic voltammetry (CV), using ferrocene as the internal standard. This series of emitters all exhibit apparent oxidation and reduction processes (Table 3 and Fig. S9, ESI†). In the cathodic scan, the reduction process with potential ranging from *ca.* −1.6 V to −1.7 V can be attributed to the reduction of the PhFIOP moiety. Meanwhile, the electron-donors contribute to the emergence of an obvious reversible oxidation process during the anodic scan. For **FIOP-*o*-Ad**/**FIOP-*o*-2Ad** and **FIOP-*o*-Cz**/**FIOP-*o*-2Cz**, they have oxidation potentials (E_{pa}) from *ca.* 0.7 V to 1.0 V, which is ascribed to the oxidation of acridine and carbazole units, respectively. However, the oxygen atom makes the phenoxazine group more susceptible to oxidation, so the E_{pa} of **FIOP-*o*-Oz**/**FIOP-*o*-2Oz** is lower than that of other emitters.

Table 3 Redox properties of these PhFIOP-based emitters

Compound	E_{pa} (V)	E_{pc} (V)	E_{HOMO}[b] (eV)	E_{LUMO}[c] (eV)	E_g^{CV}[d] (eV)
FIOP-*o*-Oz	0.53[a]	−1.61[a]	−5.34	−3.19	2.15
FIOP-*o*-Ad	0.74[a]	−1.56[a]	−5.54	−3.24	2.30
FIOP-*o*-Cz	1.03[a]	−1.75[a]	−5.83	−3.05	2.78
FIOP-*o*-2Oz	0.58[a]	−1.70[a]	−5.38	−3.10	2.28
FIOP-*o*-2Ad	0.69[a]	−1.67[a]	−5.49	−3.13	2.36
FIOP-*o*-2Cz	1.02[a]	−1.62[a]	−5.82	−3.18	2.64

[a] Reversible. The value was set as $E_{1/2}$. [b] $E_{HOMO} = -(4.8 + E_{pa})$ eV. [c] $E_{LUMO} = -(4.8 + E_{pc})$ eV. [d] CV energy gap E_g^{CV} = LUMO–HOMO.

Electroluminescence ability

To investigate the EL performance of these two TADF emitters, multilayer OLED devices were fabricated with the structure of

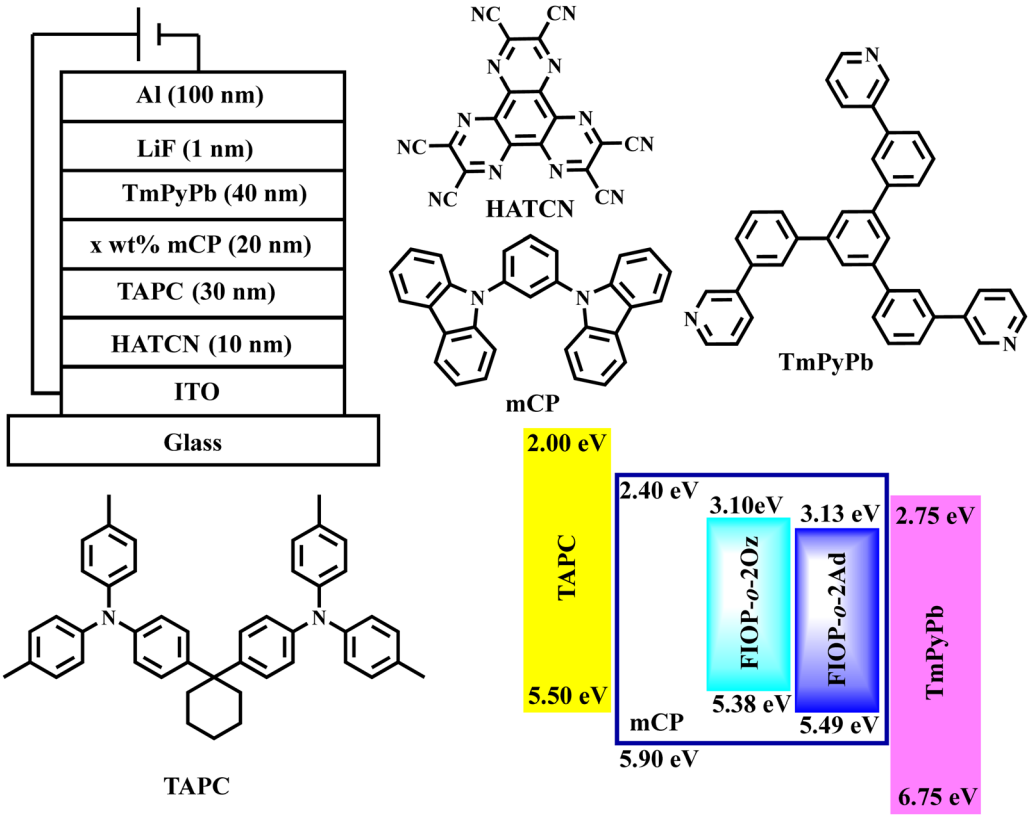

Dopant	Devices and doping level
FIOP-*o*-2Oz	A1 (6 wt%), A2 (8 wt%), A3 (10 wt%)
FIOP-*o*-2Ad	B1 (6 wt%), B2 (8 wt%), B3 (10 wt%)

Fig. 6 Device structure of the vacuum-evaporated OLEDs together with the energy-level diagram and molecular structures of the materials employed in the fabricated OLEDs.

ITO/HATCN (10 nm)/TAPC (30 nm)/*x*-wt% Emitter: mCP (20 nm)/TmPyPb (40 nm)/LiF (1 nm)/Al (100 nm) (Fig. 6). 1,4,5,8,9,11-Hexaazatriphenylenehexacarbonitrile (HATCN) and 1,1-bis[(di-4-tolylamino)phenyl]cyclohexane (TAPC) were used as the hole-injection layer and hole-transporting material, respectively. mCP serves as the host material and 1,3,5-tris(3-pyridyl-3-phenyl)benzene (TmPyPb) acts as the electron-transporting layer, whereas LiF and Al are used as the election-injection layer and cathode, respectively.

When a suitable voltage is applied to the OLEDs, the device based on **FIOP-*o*-2Oz** exhibits sky-blue EL with a maximum wavelength located at 500 nm. As for the device of **FIOP-*o*-2Ad**, blue emission with a maximum EL wavelength at 444 nm is achieved (Fig. 7a). It is worth highlighting that this is the first blue TADF emitter based on the PhFIOP acceptor reported so far, demonstrating the great potential in the construction of new TADF molecules. In addition, their EL spectra are well consistent with the PL spectra of the emitters in the mCP films, indicating that the EL signal is from the PhFIOP-based emitters. Current density–voltage–luminance (*J*–*V*–*L*) characteristic and relationship of efficiency-luminance of the devices are depicted in Fig. 7 and in the ESI† (Fig. S10 and S11). The key EL data are listed in Table 4.

As can be observed in Table 4, all devices possess a low turn-on voltage at *ca.* 3.0 V, which indicates the reasonableness of the device structure. With the doping concentration at 8 wt%, the devices achieve the optimal EL performance. The device based on **FIOP-*o*-2Oz** achieves the maximum luminance of 14139 cd m^{-2} at 18.5 V, with the maximum η_L of 55.6 cd A^{-1}, η_P of 49.2 lm W^{-1}, and η_{ext} of 27.3%. When **FIOP-*o*-2Ad** is employed as the guest emitter, the optimized device **B2** reaches the maximum luminance of 6273 cd m^{-2} at 18.0 V, the maximum η_L of 18.7 cd A^{-1}, η_P of 15.6 lm W^{-1}, and η_{ext} of 21.9% with blue emission at CIE (0.17, 0.14). The EL efficiency of the devices is slightly inferior when the doping concentration is 6 wt% or 10 wt%, but still at a high level overall. To our best knowledge, among the blue TADF emitters reported to date, the EL efficiencies of these emitters are obviously at a high level.[59–61] These results indicate that all these PhFIOP-based emitters possess excellent potential for EL applications. The reason for the high EL properties may be due to their high PLQYs (65.6% for **FIOP-*o*-2Oz** and 96.5% for **FIOP-*o*-2Ad**). In addition, the superior EL performance of **FIOP-*o*-2Oz** can be attributed to the high horizontal orientation ratio (Θ *ca.* 80%) of its transition dipole (Fig. S12, ESI†), which can result in a high η_{ext} of 27.3%. Encouragingly, both optimized devices **A2** and **B2**

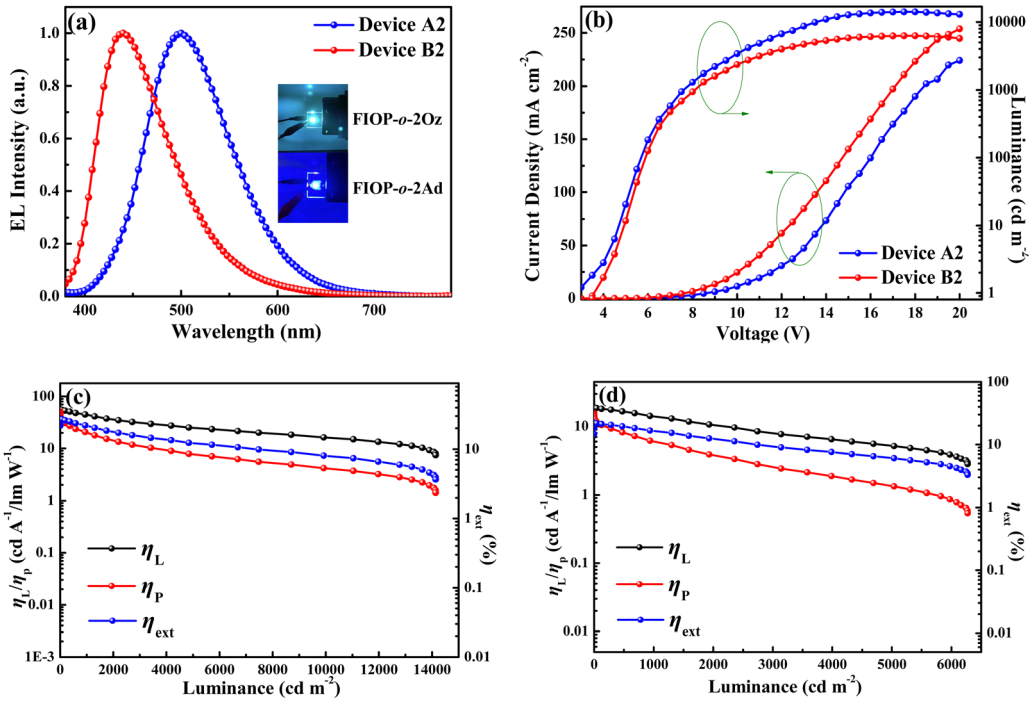

Fig. 7 (a) EL spectra of device **A2** and device **B2.** (b) Current density–voltage–luminance (*J*–*V*–*L*) characteristics for the optimized devices. Relationship between EL efficiencies and luminance of (c) device **A2**, and (d) device **B2**.

Table 4 EL Performance of the monochromatic OLEDs

Device	Dopant	$V_{turn\text{-}on}$ (V)	Luminance L_{max}[a] (cd m^{-2})	η_{ext} (%)	η_L (cd A^{-1})	η_P (lm W^{-1})	λ_{max}[d] (nm)
A1	**FIOP-*o*-2Oz** (6.0 wt%)	3.0	13129(18.0)	22.5(5.0)[a]	45.8(5.0)	37.3(4.0)	500 (0.22, 0.40)
				21.9[b]	44.6	25.7	
				18.3[c]	37.4	16.2	
A2	**FIOP-*o*-2Oz** (8.0 wt%)	3.0	14139(18.5)	27.3(5.0)	55.6(5.0)	49.2(3.5)	500 (0.23, 0.40)
				26.3	53.4	30.7	
				20.4	41.4	17.8	
A3	**FIOP-*o*-2Oz** (10.0 wt%)	3.0	9252(18.5)	18.3(4.5)	37.3(4.5)	35.9(3.5)	500 (0.23, 0.40)
				16.2	32.9	15.2	
				13.7	28.0	10.2	
B1	**FIOP-*o*-2Ad** (6.0 wt%)	3.5	5023(18.0)	10.1(6.5)	8.6(6.5)	5.7(5.5)	444 (0.16, 0.14)
				9.8	8.4	4.6	
				8.4	7.2	2.8	
B2	**FIOP-*o*-2Ad** (8.0 wt%)	3.5	6273(18.0)	21.9(5.0)	18.7(5.0)	15.6(4.0)	444 (0.17, 0.14)
				21.2	18.1	10.4	
				15.3	13.0	5.3	
B3	**FIOP-*o*-2Ad** (10.0 wt%)	3.5	5631(17.5)	18.1(4.0)	15.5(4.0)	15.3(3.5)	444 (0.16, 0.15)
				15.8	13.4	8.4	
				10.6	9.1	3.6	

[a] Maximum EL efficiency, corresponding driving voltage in brackets. [b] EL efficiency at *ca.* 100 cd m^{-2}. [c] EL efficiency at *ca.* 1000 cd m^{-2}. [d] Maximum emission wavelength and CIE color coordinates at 10 V.

possess relatively low efficiency roll-offs. For device **A2**, the η_{ext} remains 26.3% at 100 cd A^{-1} and 20.4% at 1000 cd A^{-1}, corresponding to roll-offs of 3.7% and 25.3%, respectively. Furthermore, device **B2** also exhibits low efficiency roll-offs of 3.2% at 100 cd A^{-1} and 30.1% at 1000 cd A^{-1}. Apparently, the efficiency roll-off of these devices is also at a favorable level compared with the reported results.[62,63] This is due to the fact that these PhFIOP-based emitters possess a large k_{RISC} (10^6), which inhibits the triplet-involved annihilation in the devices. These promising EL data illustrate the important potential of the PhFIOP unit in the construction of efficient TADF molecules.

Conclusions

A series of blue emitters based on the 9-phenyl-9-phosphafluorene oxide (PhFIOP) moiety have been synthesized through a convenient and novel strategy with high yields and their

photophysical, thermal, electrochemical and EL properties were also intensively investigated. The results illustrate that the emitters containing two electron-donors are more likely to exhibit TADF behavior than those containing one electron-donor. Among them, emitters coupled with two phenoxazine and two acridine units as electron-donors show obvious TADF behavior with a k_{RISC} in the order of 10^6 s^{-1}. Inspired by the high PLQYs ranging from *ca.* 70% to 90% in the doped film, their OLED devices are also prepared. The sky-blue devices achieved a maximum luminance of 14139 cd m^{-2} at 18.5 V, with a maximum η_L of 55.6 cd A^{-1}, an η_P of 49.2 lm W^{-1}, and an η_{ext} of 27.3%. Moreover, blue emission with CIE (0.17, 0.14) is also accomplished, together with high EL efficiencies of 18.7 cd A^{-1}, 15.6 lm W^{-1}, and 21.9% for maximum η_L, η_P and η_{ext}, respectively. Excitingly, this is the first reported blue TADF emitter based on the PhFIOP moiety as an acceptor with high EL efficiency. These encouraging results not only illustrate the great potential of the PhFIOP group for the construction of efficient TADF molecules, but also enrich a variety of novel emitters based on aryl phosphine oxide (APO) moieties.

Author contributions

Xi Chen: contributed to the synthesis of target molecules, performed photophysical testing, conducted device optimization and data curation, and writing-original draft. Siqi Liu: contributed to the thermal stability measurement. Yuling Sun: contributed to the synthesis of key intermediates. Daokun Zhong: contributed to the synthesis of key intermediates. Zhao Feng: contributed to the cyclic voltammetry measurement. Xiaolong Yang: contributed to the theoretical calculation. Bochao Su: revised the manuscript. Yuanhui Sun: revised the manuscript. Guijiang Zhou: contributed to the implementation of this work. Bo Jiao: contributed to the implementation of this work. Zhaoxin Wu: contributed to the implementation of this work.

Conflicts of interest

There are no conflicts to declare.

Acknowledgements

This work was supported by the National Natural Science Foundation of China (21875179, 22175137, 22101221, 52161145411, 51803163 and 21572176), and the Natural Science Foundation of Shaanxi Province (2019JZ-29). The characterization assistance from the Instrument Analysis Center of Xi'an Jiaotong University and the financial support from State Key Laboratory for Mechanical Behavior of Materials are also acknowledged.

References

1 M. Auffray, D. H. Kim, J. U. Kim, F. Bencheikh, D. Kreher, Q. Zhang, A. D'Aleo, J. C. Ribierre, F. Mathevet and C. Adachi, Dithia[3.3]Paracyclophane Core: A Versatile Platform for Triplet State Fine-Tuning and through-Space TADF Emission, *Chem. – Asian J.*, 2019, **14**, 1921–1925.

2 X. K. Chen, B. W. Bakr, M. Auffray, Y. Tsuchiya, C. D. Sherrill, C. Adachi and J. L. Bredas, Intramolecular Noncovalent Interactions Facilitate Thermally Activated Delayed Fluorescence (TADF), *J. Phys. Chem. Lett.*, 2019, **10**, 3260–3268.

3 T. Hosokai, H. Nakanotani, S. Santou, H. Noda, Y. Nakayama and C. Adachi, TADF Activation by Solvent Freezing: The Role of Nonradiative Triplet Decay and Spin-Orbit Coupling in Carbazole Benzonitrile Derivatives, *Synth. Met.*, 2019, **252**, 62–68.

4 S. Y. Lee, C. Adachi and T. Yasuda, High-Efficiency Blue Organic Light-Emitting Diodes Based on Thermally Activated Delayed Fluorescence from Phenoxaphosphine and Phenoxathiin Derivatives, *Adv. Mater.*, 2016, **28**, 4626–4631.

5 H. Uoyama, K. Goushi, K. Shizu, H. Nomura and C. Adachi, Highly Efficient Organic Light-Emitting Diodes from Delayed Fluorescence, *Nature*, 2012, **492**, 234.

6 B. M. Bell, T. P. Clark, T. S. De Vries, Y. Lai, D. S. Laitar, T. J. Gallagher, J.-H. Jeon, K. L. Kearns, T. McIntire, S. Mukhopadhyay, H. Y. Na, T. D. Paine and A. A. Rachford, Boron-Based TADF Emitters with Improved OLED Device Efficiency Roll-Off and Long Lifetime, *Dyes Pigm.*, 2017, **141**, 83–92.

7 K. W. Tsai, M. K. Hung, Y. H. Mao and S. A. Chen, Solution-Processed Thermally Activated Delayed Fluorescent OLED with High EQE as 31% Using High Triplet Energy Cross-linkable Hole Transport Materials, *Adv. Funct. Mater.*, 2019, **29**, 1901025.

8 W. Zeng, H. Y. Lai, W. K. Lee, M. Jiao, Y. J. Shiu, C. Zhong, S. Gong, T. Zhou, G. Xie, M. Sarma, K. T. Wong, C. C. Wu and C. Yang, Achieving Nearly 30% External Quantum Efficiency for Orange-Red Organic Light Emitting Diodes by Employing Thermally Activated Delayed Fluorescence Emitters Composed of 1,8-Naphthalimide-Acridine Hybrids, *Adv. Mater.*, 2018, **30**, 1704961.

9 F. B. Dias, J. Santos, D. R. Graves, P. Data, R. S. Nobuyasu, M. A. Fox, A. S. Batsanov, T. Palmeira, M. N. Berberan-Santos, M. R. Bryce and A. P. Monkman, The Role of Local Triplet Excited States and D-A Relative Orientation in Thermally Activated Delayed Fluorescence: Photophysics and Devices, *Adv. Sci.*, 2016, **3**, 1600080.

10 Y. Xiang, Z. L. Zhu, D. Xie, S. Gong, K. Wu, G. Xie, C. S. Lee and C. Yang, Revealing the New Potential of an Indandione Unit for Constructing Efficient Yellow Thermally Activated Delayed Fluorescence Emitters with Short Emissive Lifetimes, *J. Mater. Chem. C*, 2018, **6**, 7111–7118.

11 S. Wang, Y. Miao, X. Yan, K. Ye and Y. Wang, A Dibenzo-[a,C]Phenazine-11,12-Dicarbonitrile (Dbpzdcn) Acceptor Based Thermally Activated Delayed Fluorescent Compound for Efficient near-Infrared Electroluminescent Devices, *J. Mater. Chem. C*, 2018, **6**, 6698–6704.

12 Y. Kato, H. Sasabe, Y. Hayasaka, Y. Watanabe, H. Arai and J. Kido, A Sky Blue Thermally Activated Delayed Fluorescence Emitter to Achieve Efficient White Light Emission

through in Situ Metal Complex Formation, *J. Mater. Chem. C*, 2019, **7**, 3146–3149.

13 S. Chen, P. Zeng, W. Wang, X. Wang, Y. Wu, P. Lin and Z. Peng, Naphthalimide–Arylamine Derivatives with Aggregation Induced Delayed Fluorescence for Realizing Efficient Green to Red Electroluminescence, *J. Mater. Chem. C*, 2019, **7**, 2886–2897.

14 M. Chapran, P. Pander, M. Vasylieva, G. Wiosna-Salyga, J. Ulanski, F. B. Dias and P. Data, Realizing 20% External Quantum Efficiency in Electroluminescence with Efficient Thermally Activated Delayed Fluorescence from an Exciplex, *ACS Appl. Mater. Interfaces*, 2019, **11**, 13460–13471.

15 T. Hofbeck, U. Monkowius and H. Yersin, Highly Efficient Luminescence of Cu(I) Compounds: Thermally Activated Delayed Fluorescence Combined with Short-Lived Phosphorescence, *J. Am. Chem. Soc.*, 2015, **137**, 399–404.

16 P. Ganesan, W. Y. Hung, J. Y. Tso, C. L. Ko, T. H. Wang, P. T. Chen, H. F. Hsu, S. H. Liu, G. H. Lee, P. T. Chou, K. Jen Alex and Y. Chi, Functional Pyrimidinyl Pyrazolate Pt(II) Complexes: Role of Nitrogen Atom in Tuning the Solid-State Stacking and Photophysics, *Adv. Funct. Mater.*, 2019, **29**, 1900923.

17 C. H. Yang, Y. M. Cheng, Y. Chi, C. J. Hsu, F. C. Fang, K. T. Wong, P. T. Chou, C. H. Chang, M. H. Tsai and C. C. Wu, Blue-Emitting Heteroleptic Iridium(III) Complexes Suitable for High-Efficiency Phosphorescent OLEDs, *Angew. Chem., Int. Ed.*, 2007, **46**, 2418–2421.

18 W. Yang, N. Li, J. Miao, L. Zhan, S. Gong, Z. Huang and C. Yang, Simple Double Hetero[5]Helicenes Realize Highly Efficient and Narrowband Circularly Polarized Organic Light-Emitting Diodes, *CCS Chem.*, 2022, **4**, 3463–3471.

19 X. Cao, K. Pan, J. Miao, X. Lv, Z. Huang, F. Ni, X. Yin, Y. Wei and C. Yang, Manipulating Exciton Dynamics toward Simultaneous High-Efficiency Narrowband Electroluminescence and Photon Upconversion by a Selenium-Incorporated Multiresonance Delayed Fluorescence Emitter, *J. Am. Chem. Soc.*, 2022, **144**, 22976–22984.

20 Y. X. Hu, J. S. Miao, T. Hua, Z. Y. Huang, Y. Y. Qi, Y. Zou, Y. T. Qiu, H. Xia, H. Liu, X. S. Cao and C. Y. Yang, Efficient Selenium-Integrated Tadf OLEDs with Reduced Roll-Off, *Nat. Photonics*, 2022, **16**, 803–810.

21 Z. Wu, Q. Zhang, X. Wang, K. Zhang, X. Li, Q. Mu, Y. Song, J. Fan, C. K. Wang and L. Lin, Theoretical Study and Molecular Design of Thermally Activated Delayed Fluorescence Molecules Based on Intramolecular-Locked Strategy, *J. Lumin.*, 2022, **251**, 119263.

22 X. H. Zhao, C. B. Duan, X. Ma, G. D. Zou, J. Zhang, H. Xu, L. H. Xie, S. D. Yuan, Y. J. Yang and W. Huang, The Coordinated Tunning Optical, Electrical and Thermal Properties of Spiro-Configured Phenyl Acridophopsphine Oxide and Sulfide for Host Materials, *Org. Electron.*, 2021, **95**, 106193.

23 T. T. Bui, F. Goubard, M. Ibrahim-Ouali, D. Gigmes and F. Dumur, Recent Advances on Organic Blue Thermally Activated Delayed Fluorescence (TADF) Emitters for Organic Light-Emitting Diodes (OLEDs), *Beilstein J. Org. Chem.*, 2018, **14**, 282–308.

24 D. Kelly, L. G. Franca, K. Stavrou, A. Danos and A. P. Monkman, Laplace Transform Fitting as a Tool to Uncover Distributions of Reverse Intersystem Crossing Rates in TADF Systems, *J. Phys. Chem. Lett.*, 2022, **13**, 6981–6986.

25 V. Jankus, P. Data, D. Graves, C. McGuinness, J. Santos, M. R. Bryce, F. B. Dias and A. P. Monkman, Highly Efficient TADF OLEDs: How the Emitter-Host Interaction Controls Both the Excited State Species and Electrical Properties of the Devices to Achieve near 100% Triplet Harvesting and High Efficiency, *Adv. Funct. Mater.*, 2014, **24**, 6178–6186.

26 M. Y. Wong and E. Zysman-Colman, Purely Organic Thermally Activated Delayed Fluorescence Materials for Organic Light-Emitting Diodes, *Adv. Mater.*, 2017, **29**, 1605444.

27 D. Chen, X. Cai, X. L. Li, Z. He, C. Cai, D. Chen and S. J. Su, Efficient Solution-Processed Red All-Fluorescent Organic Light-Emitting Diodes Employing Thermally Activated Delayed Fluorescence Materials as Assistant Hosts: Molecular Design Strategy and Exciton Dynamic Analysis, *J. Mater. Chem. C*, 2017, **5**, 5223–5231.

28 X. Cao, D. Zhang, S. Zhang, Y. Tao and W. Huang, Cn-Containing Donor–Acceptor-Type Small-Molecule Materials for Thermally Activated Delayed Fluorescence Oleds, *J. Mater. Chem. C*, 2017, **5**, 7699–7714.

29 T. Huang, W. Jiang and L. Duan, Recent Progress in Solution Processable Tadf Materials for Organic Light-Emitting Diodes, *J. Mater. Chem. C*, 2018, **6**, 5577–5596.

30 D. G. Chen, T. C. Lin, C. L. Chen, Y. L. Chen, Y. A. Chen, G. H. Lee, P. T. Chou, C. W. Liao, P. C. Chiu, C. H. Chang, Y. J. Lien and C. Yun, Optically Triggered Planarization of Boryl-Substituted Phenoxazine: Another Horizon of Tadf Molecules and High-Performance OLEDs, *ACS Appl. Mater. Interfaces*, 2018, **10**, 12886–12896.

31 M. Hirai, N. Tanaka, M. Sakai and S. Yamaguchi, Structurally Constrained Boron-, Nitrogen-, Silicon-, and Phosphorus-Centered Polycyclic Pi-Conjugated Systems, *Chem. Rev.*, 2019, **119**, 8291–8331.

32 J. Li, D. Ding, Y. Wei, J. Zhang and H. Xu, A ''Si-Locked'' Phosphine Oxide Host with Suppressed Structural Relaxation for Highly Efficient Deep-Blue TADF Diodes, *Adv. Opt. Mater.*, 2016, **4**, 522–528.

33 B. Wang, X. Lv, B. Pan, J. Tan, J. Jin and L. Wang, Benzimidazole–Phosphine Oxide Hybrid Electron Transporters for Unilateral Homogeneous Phosphorescent Organic Light-Emitting Diodes with Enhanced Power Efficiency, *J. Mater. Chem. C*, 2015, **3**, 11192–11201.

34 Z. Yang, Z. Mao, Z. Xie, Y. Zhang, S. Liu, J. Zhao, J. Xu, Z. Chi and M. P. Aldred, Recent Advances in Organic Thermally Activated Delayed Fluorescence Materials, *Chem. Soc. Rev.*, 2017, **46**, 915–1016.

35 L. Bergmann, D. M. Zink, S. Brase, T. Baumann and D. Volz, Metal-Organic and Organic TADF-Materials: Status, Challenges and Characterization, *Top. Curr. Chem.*, 2016, **374**, 22.

36 K. Duan, D. Wang, M. Yang, Z. Liu, C. Wang, T. Tsuboi, C. Deng and Q. Zhang, Weakly Conjugated Phosphine Oxide Hosts for Efficient Blue Thermally Activated Delayed

Fluorescence Organic Light-Emitting Diodes, *ACS Appl. Mater. Interfaces*, 2020, **12**, 30591–30599.

37 B. Sk, V. Thangaraji, N. Yadav, G. P. Nanda, S. Das, P. Gandeepan, E. Zysman-Colman and P. Rajamalli, High Performance Non-Doped Green Organic Light Emitting Diodes Via Delayed Fluorescence, *J. Mater. Chem. C*, 2021, **9**, 15583–15590.

38 C. W. Lee and J. Y. Lee, Comparison of Tetraphenylmethane and Tetraphenylsilane as Core Structures of High-Triplet-Energy Hole- and Electron-Transport Materials, *Chem. Eur. J.*, 2012, **18**, 6457–6461.

39 C. Han, Z. Zhang, D. Ding and H. Xu, Dipole–Dipole Interaction Management for Efficient Blue Thermally Activated Delayed Fluorescence Diodes, *Chem*, 2018, **4**, 2154–2167.

40 M. Colella, P. Pander, D. S. Pereira and A. P. Monkman, Interfacial TADF Exciplex as a Tool to Localize Excitons, Improve Efficiency, and Increase OLED Lifetime, *ACS Appl. Mater. Interfaces*, 2018, **10**, 40001–40007.

41 G. Mallesham, C. Swetha, S. Niveditha, M. E. Mohanty, N. J. Babu, A. Kumar, K. Bhanuprakash and V. J. Rao, Phosphine Oxide Functionalized Pyrenes as Efficient Blue Light Emitting Multifunctional Materials for Organic Light Emitting Diodes, *J. Mater. Chem. C*, 2015, **3**, 1208–1224.

42 J. Lee, N. Aizawa and T. Yasuda, Molecular Engineering of Phosphacycle-Based Thermally Activated Delayed Fluorescence Materials for Deep-Blue OLEDs, *J. Mater. Chem. C*, 2018, **6**, 3578–3583.

43 C. Fan, Y. Li, C. Yang, H. Wu, J. Qin and Y. Cao, Phosphoryl/Sulfonyl-Substituted Iridium Complexes as Blue Phosphorescent Emitters for Single-Layer Blue and White Organic Light-Emitting Diodes by Solution Process, *Chem. Mater.*, 2012, **24**, 4581–4587.

44 H. Yang, Q. Liang, C. Han, J. Zhang and H. Xu, A Phosphanthrene Oxide Host with Close Sphere Packing for Ultralow-Voltage-Driven Efficient Blue Thermally Activated Delayed Fluorescence Diodes, *Adv. Mater.*, 2017, **29**, 1700553.

45 X. Ban, T. Zhou, Q. Cao, K. Zhang, Z. Tong, H. Xu, A. Zhu and W. Jiang, Combining Molecular Encapsulation and an AIE Strategy to Construct an Efficient Blue TADF Polymer for Solution-Processed Multilayer White OLEDs, *J. Mater. Chem. C*, 2022, **10**, 15114–15125.

46 C. Duan, Y. Xin, Z. Wang, J. Zhang, C. Han and H. Xu, High-Efficiency Hyperfluorescent White Light-Emitting Diodes Based on High-Concentration-Doped TADF Sensitizer Matrices Via Spatial and Energy Gap Effects, *Chem. Sci.*, 2021, **13**, 159–169.

47 Z. Li, C. Duan, Y. Li, J. Zhang, C. Han and H. Xu, Exciton Engineering Based on Star-Shaped Blue Thermally Activated Delayed Fluorescence Emitters for Efficient White Organic Light-Emitting Diodes, *J. Mater. Chem. C*, 2021, **9**, 15221–15229.

48 J. Zhang, J. Sun, Y. Ma, C. Han, D. Ding, Y. Wei and H. Xu, Multiplying Phosphine-Oxide Orientation to Enable Ultralow-Voltage-Driving Simple White Thermally Activated Delayed Fluorescence Diodes with Power Efficiency over 100 lm^{-1}, *Adv. Funct. Mater.*, 2022, 2209163.

49 D. Zhong, Y. Yu, L. Yue, X. Yang, L. Ma, G. Zhou and Z. Wu, Optimizing Molecular Rigidity and Thermally Activated Delayed Fluorescence (TADF) Behavior of Phosphoryl Center Π-Conjugated Heterocycles-Based Emitters by Tuning Chemical Features of the Tether Groups, *Chem. – Eur. J.*, 2021, **413**, 127445.

50 D. Zhong, Y. Yu, D. Song, X. Yang, Y. Zhang, X. Chen, G. Zhou and Z. Wu, Organic Emitters with a Rigid 9-Phenyl-9-Phosphafluorene Oxide Moiety as the Acceptor and Their Thermally Activated Delayed Fluorescence Behavior, *ACS Appl. Mater. Interfaces*, 2019, **11**, 27112–27124.

51 I. S. Park, S. Y. Lee, C. Adachi and T. Yasuda, Full-Color Delayed Fluorescence Materials Based on Wedge-Shaped Phthalonitriles and Dicyanopyrazines: Systematic Design, Tunable Photophysical Properties, and OLED Performance, *Adv. Funct. Mater.*, 2016, **26**, 1813–1821.

52 Y. Kitamoto, T. Namikawa, D. Ikemizu, Y. Miyata, T. Suzuki, H. Kita, T. Sato and S. Oi, Light Blue and Green Thermally Activated Delayed Fluorescence from 10h-Phenoxaborin-Derivatives and Their Application to Organic Light-Emitting Diodes, *J. Mater. Chem. C*, 2015, **3**, 9122–9130.

53 S. H. Lee, C. T. Chan, K. M. Wong, W. H. Lam, W. M. Kwok and V. W. Yam, Design and Synthesis of Bipyridine Platinum(II) Bisalkynyl Fullerene Donor-Chromophore-Acceptor Triads with Ultrafast Charge Separation, *J. Am. Chem. Soc.*, 2014, **136**, 10041–10052.

54 J. A. Christensen, B. T. Phelan, S. Chaudhuri, A. Acharya, V. S. Batista and M. R. Wasielewski, Phenothiazine Radical Cation Excited States as Super-Oxidants for Energy-Demanding Reactions, *J. Am. Chem. Soc.*, 2018, **140**, 5290–5299.

55 M. Onoda, Y. Koyanagi, H. Saito, M. Bhanuchandra, Y. Matano and H. Yorimitsu, Synthesis of Dibenzophosphole Oxides from Dibenzothiophene Dioxides and Phenylphosphine by Two Successive SnAr Reactions, *Asian J. Org. Chem.*, 2017, **6**, 257–261.

56 Y. Kurimoto, J. Yamashita, K. Mitsudo, E. Sato and S. Suga, Electrosynthesis of Phosphacycles Via Dehydrogenative C-P Bond Formation Using Dabco as a Mediator, *Org. Lett.*, 2021, **23**, 3120–3124.

57 A. Kaga, H. Iida, S. Tsuchiya, H. Saito, K. Nakano and H. Yorimitsu, Aromatic Metamorphosis of Thiophenes by Means of Desulfurative Dilithiation, *Chem. – Eur. J.*, 2021, **27**, 4567–4572.

58 W. Zhao, W. Yang, R. Li and C. Li, Homogeneous Palladium-Catalyzed Selective Reduction of 2,2′-Biphenols Using Hco2h as Hydrogen Source, *Synthesis*, 2020, 1605–1618.

59 J. Wang, N. Li, Q. Chen, Y. Xiang, X. Zeng, S. Gong, Y. Zou and Y. Liu, Triarylboron-Cored Multi-Donors TADF Emitter with High Horizontal Dipole Orientation Ratio Achieving High Performance OLEDs with near 39% External Quantum Efficiency and Small Efficiency Roll-Off, *Chem. – Eur. J.*, 2022, **450**, 137805.

60 Y. Zhu, S. Zeng, W. Gong, X. Chen, C. Xiao, H. Ma, W. Zhu, J. Yeob Lee and Y. Wang, Molecular Design of Blue Thermally Activated Delayed Fluorescent Emitters for High

Efficiency Solution Processable OLED Via an Intramolecular Locking Strategy, *Chem. – Eur. J.*, 2022, **450**, 138459.
61 M. W. Cooper, X. Zhang, Y. Zhang, A. Ashokan, C. Fuentes-Hernandez, S. Salman, B. Kippelen, S. Barlow and S. R. Marder, Delayed Luminescence in 2-Methyl-5-(Penta(9-Carbazolyl)Phenyl)-1,3,4-Oxadiazole Derivatives, *J. Phys. Chem. A*, 2022, **126**, 7480–7490.
62 J. Huo, S. Xiao, Y. Wu, M. Li, H. Tong, H. Shi, D. Ma and B. Z. Tang, Molecular Engineering of Blue Diphenylsulfone-Based Emitter with Aggregation-Enhanced Emission and Thermally Activated Delayed Fluorescence Characteristics: Impairing Intermolecular Electron-Exchange Interactions Using Steric Hindrance, *Chem. Eng. J.*, 2023, **452**, 138957.
63 Y. Yu, P. Xu, Y. Pan, X. Qiao, L. Ying, D. Hu, D. Ma and Y. Ma, Pyrene-Based Emitters with Ultrafast Upper-Level Triplet-Singlet Intersystem Crossing for High-Efficiency, Low Roll-Off Blue Organic Light-Emitting Diode, *Adv. Opt. Mater.*, 2023, **11**, 2202217.

